New Journal of Physics
The open-access journal for physics

Electrokinetic control of sample splitting at a channel bifurcation using isotachophoresis

Alexandre Persat and Juan G Santiago[1]
Department of Mechanical Engineering, Stanford University, Stanford, CA 94305, USA
E-mail: juan.santiago@stanford.edu

New Journal of Physics **11** (2009) 075026 (15pp)
Received 28 January 2009
Published 31 July 2009
Online at http://www.njp.org/
doi:10.1088/1367-2630/11/7/075026

Abstract. We present a novel method for accurately splitting ionic samples at microchannel bifurcations. We leverage isotachophoresis (ITP) to focus and transport sample through a one-inlet, two-outlet microchannel bifurcation. We actively control the proportion of splitting by controlling potentials at end-channel reservoirs (and thereby controlling the current ratio). We explore the effect of buffer chemistry and local electric field on splitting dynamics and propose and validate a simple Kirchoff-type rule controlling the split ratio. We explore the effects of large applied electric fields on sample splitting and attribute a loss of splitting accuracy to electrohydrodynamic instabilities. We propose a scaling analysis to characterize the onset of this instability. This scaling is potentially useful for other electrokinetic flow problems with self-sharpening interfaces.

[1] Author to whom any correspondence should be addressed.

Contents

1. Introduction

Microfluidic platforms provide new tools to contemporary chemical and biological sciences. Microfluidic devices are often an effective alternative to traditional methods, particularly when analyzing small sample volumes. A current challenge of microfluidics is its application to high throughput and parallel analyses required by complex and multiple samples. Significantly parallel microfluidic assays such as microchannel networks [1]–[3] and separation channel arrays [4, 5] are working to address this.

The splitting of a single zone into two or more distinct sample zones is a basic and recurring function of a wide variety of microfluidic systems, including both single- and two-phase flow devices. For example, Adamson *et al* [6] showed drop splitting at successive T-junctions for generation of sample zone arrays; in the same manner Link *et al* [7] used a unique T-junction to control plug size after splitting. Roman *et al* [8] used a K-shaped channel intersection to sample a small volume of a drop in a segmented flow-type device, with subsequent electrophoretic separation. Such sample control and partition is also common in two-dimensional (2D) assay systems. For example, Das *et al* [9] separated protein species along a primary isoelectric focusing channel and then divided the separated species into an array of 29 parallel channels for subsequent capillary gel electrophoresis. Griffiths and Nilson [10] optimized channel junctions to minimize sample dispersion during electrophoretic splitting. Recently, Zhuang and Jacobson [11] were able to interface a unique sample loading channel to three parallel separation channels. Together, these various techniques have the potential to simplify sample loading for multidimensional separation and binding assays.

There remain key challenges in achieving accurate and repeatable sample splitting. For example, Adamson *et al* [6] pointed out that back pressure causes asymmetry in sample splitting in their system, where droplet lengths vary significantly at flow rates below $40\,\mu\mathrm{l\,min}^{-1}$ in their device. Despite the accuracy of their electrokinetic flow control system, Zhuang and Jacobson [11] pointed out that their serial-to-parallel injection scheme increases peak width, adversely impacting resolution in subsequent electrokinetic separations. Also, potential sample leak limits the number of parallel separation channels.

We here present a technique that can be used to split samples at channel bifurcations, while minimizing sample zone dispersion. We leverage isotachophoresis (ITP) to focus and control

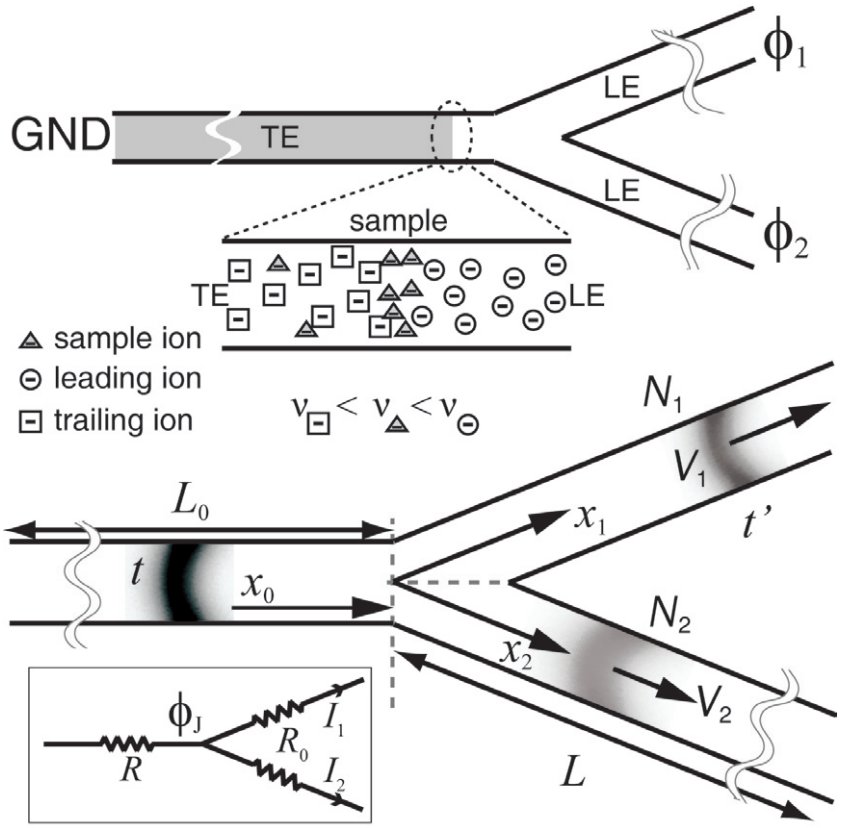

Figure 1. Schematic of the anionic ITP splitting experiment. Initially, the channels are filled with LE. The inlet channel reservoir contains TE and sample. Upon application of an electric field, ionic species self-segregate into three zones (generally in order of increasing electrophoretic mobility v): trailing ion, sample ion and leading ion. ITP focusing generates a sharp sample zone between TE and LE. The interface propagates toward the channel bifurcation. The bottom schematic shows (actual images of) a splitting of the sample zone. Before bifurcation, (here time t), the sample is in the inlet channel (length L_0, axial coordinate x_0). After splitting, sample zones enter channels 1 and 2 (length L, axial coordinates x_1 and x_2). The quantity of sample in channel i is N_i and the associated sample zone velocity is V_i. The inset at the bottom left shows the equivalent circuit. The electric resistance of respectively the inlet channel and bifurcation channels are R and R_0. The potential at the junction is ϕ_J and current in branch i is I_i.

the sample and protect it from dispersion as it divides into two distinct sample zones in a Y-shaped bifurcation channel geometry. ITP is a robust electrophoretic preconcentration technique leveraging strong electric field gradients that protect focused samples from dispersion [12]. In ITP, ionic sample species focus and separate based on their electrophoretic mobilities between the leading ions and trailing ions as illustrated in figure 1. There is abundant literature discussing the physics of ITP [13]–[16], and numerous and diverse applications such as sample preconcentration [17, 18], measurement of dissociation constants [19], sensitive

analyte separation and detection [20, 21]. In the current work, we control applied electric potentials at the end of each junction channel to accurately split a sample zone focused by ITP. We show the ITP bifurcation technique is accurate across buffer chemistries and a wide range of electric fields. We propose and validate simple scaling laws that can be used to predict and control the splitting ratio and velocity of sample zones at intersections. We also show that there is a practical upper limit on the electric field (and conductivity ratio) for accurate sample splitting. Namely, we observe and document the effects of flow instabilities on the flow and bifurcation dynamics and the precision of the split.

2. Theory

The physics associated with the current unsteady electrohydrodynamic problem are quite complex. As discussed by Saville and Palusinski [22], ITP systems involve the coupled convective–diffusion–reaction transport equations of multiple species. Calculation of the electric field near the interface is complicated by high and unsteady conductivity gradients [23]. Also involved are the effects of non-uniform, unsteady electroosmosis on fluid flow and conductivity fields [24]. Further, the near-bifurcation geometry of interest here is fully three-dimensional.

Despite the challenges of physics-based modeling from first principles, we can hypothesize some simple relations describing the split of ITP zones migrating through bifurcation geometry. We consider several simplifications of the flow. First, we apply Kirchoff's law for current conservation relating voltage drops in the inlet and outlet channels. To do this, we approximate the ITP interface containing sample as an abrupt change in the conductivity. This is true when the width of the diffuse interface is much smaller than the total length of the channel, which is typically the case in ITP. In these conditions, the respective electrical resistances, R, of the TE (subscript T) and LE (subscript L) zones are $R_\mathrm{T} = L_\mathrm{T}/(A\sigma_\mathrm{T})$ and $R_\mathrm{L} = L/(A\sigma_\mathrm{L})$ where L and σ are, respectively, the length and conductivity of the zone, and A is the channel cross-sectional area. Note that σ_T is the conductivity of the adapted TE (i.e. the TE occupying regions formerly occupied by LE) [12]. When the LE/TE interface first reaches the intersection, the upstream channel contains TE only and each downstream branch contains LE only. For potentials ϕ_1 and ϕ_2 applied, respectively, at the ends of channels 1 and 2, we find the approximate potential at the junction

$$\phi_\mathrm{J} = \frac{\phi_1 + \phi_2}{R/R_0 + 2} = \frac{\phi_1 + \phi_2}{\gamma^{-1}\,(L/L_0) + 2}. \tag{1}$$

Here R and R_0 are, respectively, the resistance of the upstream channel and that of one geometrically symmetric branch (cf equivalent circuit in figure 1), and conductivity ratio $\gamma = \sigma_\mathrm{L}/\sigma_\mathrm{T}$. The electric field in branch i of length L is simply $E_i = (\phi_i - \phi_\mathrm{J})/L$ and the current $I_i = \sigma_\mathrm{L} E_i A$. This current conservation at the bifurcation 'node' holds nearly exactly just before and just after the arrival and splitting of the high-gradient ITP zone. After splitting, different electric fields in the outlet branches can cause different sample zone velocities (cf figure 1) and this breaks the symmetry in the conductivity field.

Next, we know that before and after splitting of the ITP zone, the velocity and current of each of the three bifurcation legs (inlet and two outlets) can be evaluated using local 1D ITP approximations. Assuming the electroosmotic flow velocities are much smaller than electrophoretic velocities, we can relate interface velocities simply to the electric fields in the

LE of each channel branch. The drift velocity of the interface in the branch i is the velocity of the leading ion $\nu_L E_i$ (ν is the electrophoretic mobility) so that

$$V_2/V_1 = E_2/E_1. \tag{2}$$

We here hypothesize that the splitting of focused analyte molecules as they navigate the bifurcation will follow the ionic current splitting demanded by a Kirchoff node approximation. Therefore, we can write simply

$$N_2/N_1 = I_2/I_1 = E_2/E_1, \tag{3}$$

where N_1 and N_2 are, respectively, the amounts of sample (e.g. in moles) which leave the bifurcation in channels 1 and 2 (again, cf figure 1). We will experimentally validate equations (2) and (3) in the results section. We will also show that equation (3) breaks down for regimes where field strength and conductivity ratio are large enough to induce electrokinetic flow instabilities at the ITP interface; while the velocity ratio (2) holds at all of the conditions we explored.

3. Materials and methods

We prepared LE solution of Tris hydrochloride (100 mM, pH = 8.0), and TE solutions of Tris HEPES (100 mM, pH = 8.0), sodium benzoate (50 mM), taurine (100 mM) and sodium tetraphenylborate (TPB, 75 mM); salts were all purchased from Sigma (St Louis, MO). All solutions were prepared in UltraPure DNase/RNase free distilled water (GIBCO Invitrogen, Carlsbad, CA). We added 5 mM barium hydroxide to taurine TE to limit the effect of dissolved atmospheric carbon dioxide on ITP dynamics [25]. The TE contains 100 nM Alexa Fluor 488 carboxylic acid succinimidyl ester mixed isomers (excitation/emission 490/520 nm, Molecular Probes, OR) used as a simple fluorescent sample. We reduced EOF by silanizing channel walls with Sigmacote, and adding 1% polyvinylpyrrolidone (PVP, Polysciences Inc, Warrington, PA) as a dynamic coating element to all electrolyte solutions. For simplicity and ease of repeatability, we used no PVP additive in the instability study.

We used borosilicate microchips purchased from IMT (Tokyo, Japan) with 100 μm wide, 40 μm deep channels containing a Y bifurcation (models ICC-SY05 and ICC-CO01). For measurements of γ and the instability visualization of figure 4, we used a 70 μm wide, 10 μm deep straight channel (model NS33X, Caliper Life Sciences, Mountain View, CA). We measured γ and the resistance of each branch of the bifurcations via current monitoring performed with a high-voltage sourceMeter (model 2410, Keithley Instruments, Cleveland, OH). For the ITP processes, we controlled electric potential with a high-voltage power supply (Labsmith, Livermore, CA). We visualized ITP splitting and instability using an inverted epifluorescent microscope equipped with 4× (Plan APO, N.A. = 0.2), 10× (Plan APO, N.A. = 0.45) and 20× (LU APO, N.A. = 0.4) microscope objectives (Nikon, Japan), a mercury bulb (Ushio, Japan), a filter cube (exciter/emitter 485/535 nm, Omega, Brattleboro, VT) and a 0.6× demagnification lens (model RD060-CMT, Diagnostic Instruments, Sterling Heights, MI). Images were acquired with a CCD camera (Cascade 512F, Photometrics, Tucson, AZ) controlled with Winview32 software (Princeton Instruments, Trenton, NJ).

4. Results and discussion

4.1. Sample splitting at a channel bifurcation

We here present an experimental study of ITP sample zone flows through a Y-shaped bifurcation in a microchannel system. Our observations serve as a (first and) basic study of the application of ITP to preconcentrate, transport and split sample species in microchannel networks. We first demonstrate the principle of sample splitting in figure 2. Figures 2(a)–(c) show measured data for three cases of electric field ratio of the two outlet branches. The left column of figure 2 shows images of three representative ITP sample zones as they approach and split at the junction. For each composite image shown, we superposed the intensity of three images at the times indicated to capture more details of the shape and dynamics of the ITP zone. As per equation (1), we vary electric field in each channel by controlling potentials ϕ_1 and ϕ_2 as shown in figure 1 (inlet channel reservoir is always grounded). In the right-hand column of figure 2, we show three measured spatiotemporal diagrams corresponding to the three adjacent composite images. The spatiotemporal diagrams are plots of width-averaged fluorescence intensity within each of the three channel branches as a function of distance along that channel branch and time. The abscissa corresponds to the three x-axes shown in figure 1. The width averaging is performed in directions perpendicular to the centerline of each channel branch and within each channel section as defined by the dashed lines in the bottom schematic of figure 1.

For all electric field cases, ITP zones initially approach the bifurcation at approximately constant velocity. This is shown by the constant slope of the traces of the inlet channel spatiotemporal plots. As channel cross sections widen at the bifurcation inlet, we see an expected decrease in approach velocity (note the curvature of the spatiotemporal diagrams of the inlet channel). As sample zones split and leave the bifurcation, they again reach approximately constant velocities as expected for short distances in constant voltage ITP.[2] Figure 2(a) shows the case of symmetric electric fields on the outlet channels. Accordingly, the streaks in the spatiotemporal diagrams have equal slopes in the outlet channels, consistent with applied symmetric electric fields and equation (2). We see from both the images and spatiotemporal plots that the normalized outlet intensities (proportional to concentration) are approximately equal and that the outlet band shapes are symmetric and similar to that of the inlet band shape. Figures 2(b) and (c) show the effects of asymmetry in applied electric fields. In these, we see a noticeable asymmetry in the shape of the ITP zone at intermediate times (e.g. immediately before splitting); and this is accompanied by a redistribution (along the vertical direction) of molecules within the as-yet contiguous band, immediately before the split occurs. For example, note the relatively high-intensity region at the top of the $t = 1$ s image of figure 2(c). Increases in the top channel field (E_1) relative to the bottom (E_2) result in both higher intensity sample zones and higher outlet velocities in the top channel. For example, in figure 2(b) the velocity and width-averaged intensity ratios are 0.42 and 0.43, respectively, consistent with the applied electric field ratio of 0.43. Figure 2(c) shows a near-limiting case, where E_1 is sevenfold higher than E_2. Here, only a small portion of the sample enters channel 2 and the measured velocity and intensity ratios are 0.24 and 0.18, respectively (compared to $E_2/E_1 = 0.15$, although here

[2] In constant voltage ITP, the interface position determines the current in the channels and therefore the local field. However, over distances short compared to the length of the channel, the one-dimensional ITP analysis yields approximately constant velocity. The visualization region in figure 2 constitutes less than 1% of our channel lengths and so we can expect constant velocity translation.

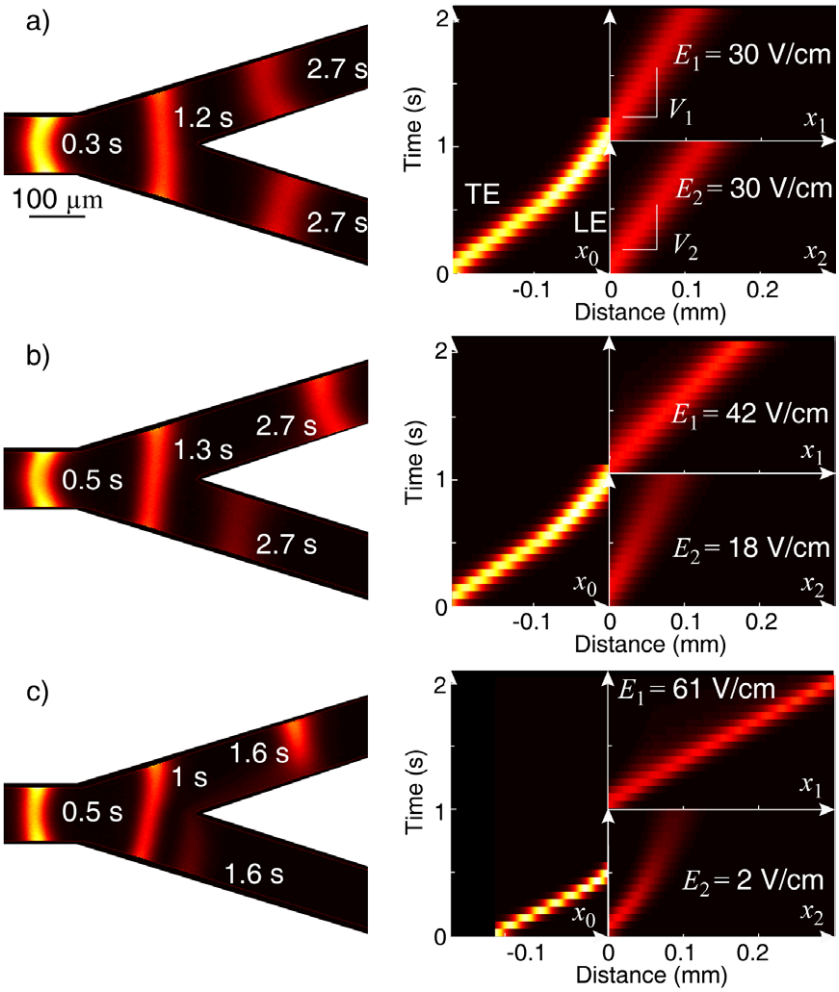

Figure 2. Experimental measurements of ITP sample splitting at a bifurcation. Here, TE is 75 mM sodium benzoate, sample is Alexa Fluor 488, and LE is 100 mM Tris hydrochloride (pH = 8.0). Left column shows composite images obtained by superposing three images per experiment. The sample zone just enters the field of view near time $t = 0$ s. The right column shows the corresponding spatiotemporal plots of width-averaged intensity versus time and distance along each of the three channels. (a) The case of equal electric field in both of the outlet channels. The sample zone migrates within the inlet channel ($t = 0.5$ s), enters the bifurcation ($t = 1.2$ s) and splits ($t = 2.7$ s). Spatiotemporal plots of outlet channels show a symmetric split with equal outlet intensities and velocities. (b) An asymmetric case with stronger electric field in the top channel. After splitting, more of the sample zone enters channel 1 than 2, and the outlet velocity in 1 is also higher. (c) A near-limiting case where electric field in 1 is 7 times larger than in 2. Here, only a small fraction enters 2, at a comparatively very low velocity.

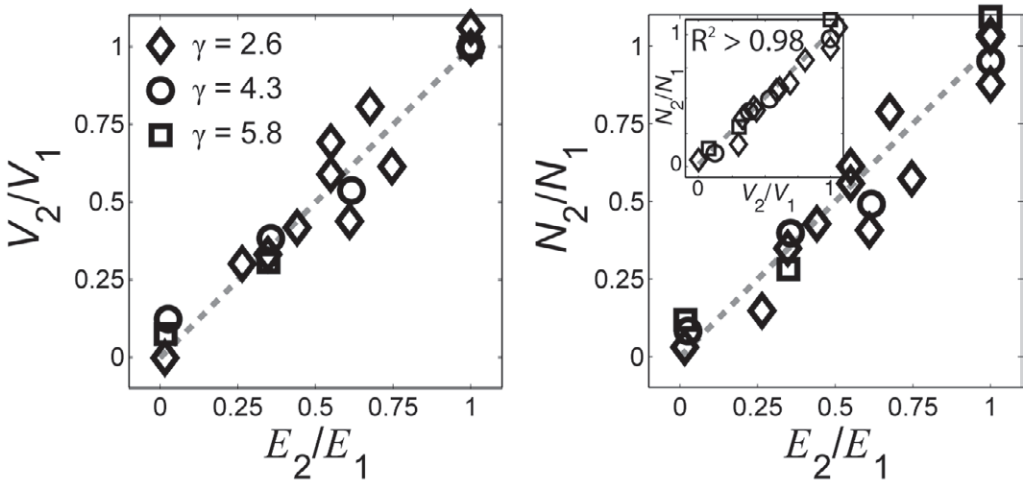

Figure 3. Velocity and splitting ratio at various electric fields ratios and TE conductivities. The electric field in the LE ranges between 1 and 60 V cm^{-1}. The velocity ratio V_2/V_1 correlates strongly with electric field ratio E_2/E_1. The sample splitting ratio N_2/N_1 also correlates with E_2/E_1. This validates the hypothesis that sample splitting follows a Kirchoff-type law; where sample splits with the same proportions as current. In the inset, we show the correlation between sample splitting ratio and velocity ratio. The latter two quantities are measured directly and show the strongest correlation. These results hold across a variety of TE chemistries including sodium benzoate ($\gamma = 2.6$), Tris HEPES ($\gamma = 4.3$) and taurine ($\gamma = 5.8$). This set of splitting experiments shows an average splitting ratio of about 0.08 (for a current ratio of 0.07).

the bottom channel has not yet reached steady state). In the next section, we present a series of quantitative comparisons of outlet splitting and velocity ratios to applied field ratio E_2/E_1.

4.2. Sample splitting and electric field ratio

We now explore the relationship between sample splitting and applied electric fields. Figure 3 summarizes typical splitting results for stable electrokinetic flows (see the next section), for various combinations of applied potentials and TE chemistries. To determine conductivity ratios, γ, for each TE, we ran preliminary ITP experiments where we monitored current to measure: (i) the initial resistance of the channel, when entirely filled with LE, and (ii) the final resistance of the channel containing only (adapted) TE. The ratio of the second to the first resistance yields γ. Consistent with the hypothesis formulated in equations (2) and (3), both velocity ratio and splitting ratio effectively scale with the electric field ratio. Due to the physics of ITP, the velocity ratio is effectively a measurement of current ratio; and so this result validates the 1D calculation of the electric field in each channel branch from equation (1). We see that the proposed scaling is insensitive to the absolute value of electric field (which varied here from 1 to 60 V cm^{-1}) and is insensitive to TE chemistry. We summarize the observed proportionality in the inset of figure 3(b), where we plot splitting ratio versus velocity ratio. We see a good correlation between these two directly measured parameters (which are therefore completely independent of any electric field or current calculations).

These results show that we can control splitting of the ITP-focused sample species fairly accurately by simply controlling end-channel reservoir electric potentials, knowing channel branch lengths and estimating the conductivity ratio between LE and adapted TE [12]. In practice, we can gain accuracy by carefully measuring the resistance of each channel (in a calibration experiment using a homogeneous buffer) to obtain an effective length ratio (yielding parameter L/L_0 of equation (1)). Figure 3 shows fairly repeatable splitting ratios from about 1.0 to 0.08.

In the rest of the paper, we describe and characterize a limitation of our splitting technique. We first describe qualitatively observed dynamics of ITP-focused sample zones in straight channels (e.g. similar to our approach channel). We then present an experimental study of the effects observed at large applied electric field on the splitting at our Y-junction. We then propose a simple scaling argument based on electrohydrodynamic instability theory to describe approximately the regime in which one should expect inaccuracy of ITP zone splitting.

4.3. ITP-focused sample fluctuations observed at high fields

We first present observations of the ITP-focused sample zone in a straight channel, with reduced EOF (without polymeric dynamic coating). In ITP, the interface between two adjoined ion zones is self-sharpening [12, 13], and typically acquires a stable steady state. Figure 4(a) shows a typical (stable) ITP-focusing experiment at an electric field of $20\,\mathrm{V\,cm^{-1}}$ where the sample eventually acquires a shape which is approximately uniformly distributed along the channel cross section.

At sufficiently high electric field, we observe spatiotemporal fluctuations of the sample zone. Figures 4(b) and (c) show flow visualizations using the same sample, TE and LE chemistries as that of 4(a), but with increasingly higher applied nominal electric fields (defined here as applied potential divided by total distance). Figure 4(b) shows one example of a composite image (here superposing six images) at $120\,\mathrm{V\,cm^{-1}}$. We see the sample zone acquires strong spanwise (normal to centerline and parallel to the image plane) gradients in sample concentration. The sample zone here loses fore-aft symmetry, and loses some of its symmetry along the centerline. Figure 4(c) shows a typical composite image at $190\,\mathrm{V\,cm^{-1}}$. At large fields, we see the sample zone shows strong fluctuations in both shape and concentration, and loses symmetry along all directions. We have observed similar fluctuations in a large number of experiments. These shape and intensity fluctuations are consistently more pronounced at higher electric fields. We have also observed a few cases where the sample zone at low electric field appeared stable with benzoate as TE ($\gamma \simeq 2.6$) and showed significant fluctuations with TPB as TE ($\gamma \simeq 9.1$), even at the same applied electric field. Given these observations, we explored the effect of the ITP fluctuations on the splitting problem. To this end, we performed experiments similar to those described in figure 1 but for increasing values of electric field and/or conductivity ratio.

4.4. Study of effects of flow instabilities on ITP zone splitting

Fluctuations at large applied electric fields in the presence of conductivity gradients are features of electrohydrodynamic (EHD) instabilities. In this part, we describe indications that strongly support that electrokinetic flow instabilities (EKI, a regime of EHD instabilities) limit the

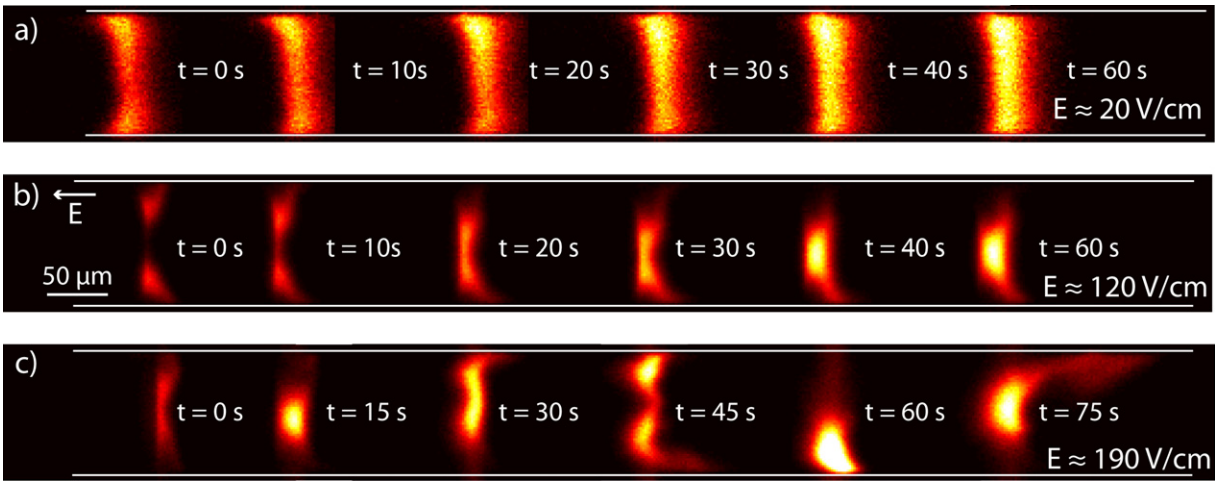

Figure 4. Composite images of ITP experiments in a straight channel with increasing electric field. TE is 100 mM Tris HEPES. We superposed successive instantaneous images of the sample zone (the relative axial position does not correspond to actual displacement). (a) Successive images of the ITP-focused sample zone at low electric field, where we observe no fluctuations. Sample zone concentration increases with time as predicted by peak-mode ITP theory [13]. The sample zone acquires a shape which is approximately uniform and symmetric along the spanwise direction. (b) The same conditions and channel, but at higher electric field. At this field, we begin to observe fluctuations in the shape and intensities of the sample zone (and the sample acquires a slight streamwise asymmetry). (c) Images of the sample at a relatively large electric field. The fluctuations of the sample zone shape and intensities are more pronounced, and the sample loses symmetry about all directions.

accuracy with which ITP sample zones can be split at large electric field and large conductivity ratios.

In classical EHD instability, electric fields couple with (orthogonal components of) conductivity gradients to generate local regions of net free charge [26, 27]. Local, net free charges can generate electric body forces, which can drive and destabilize fluid flow. Lin *et al* [28] studied EHD instabilities in the regime applicable to electrokinetic microflows; and termed this regime electrokinetic instability (EKI). There have been several other studies of EKI including Posner and Santiago's [29] study of EKI at a four-channel intersection; and more recently the work of Santos and Storey [30] who presented simulations of EKI resulting in electrokinetic flows where applied electric field is roughly parallel to streamwise conductivity gradients. The latter work considered simple binary electrolytes and a base state field consistent with field amplified sample stacking. We shall here make some observations based on the work of Posner and Santiago [29] and Santos and Storey [30], but as described by Oddy and Santiago [31], we note that non-binary, non-symmetric electrolytes (as we have in the current study) can significantly complicate EKI physics. For example, Oddy and Santiago showed that the addition of a third ionic species can reduce by two orders of magnitude the electric fields at which significant perturbation growth rates (and associated flow instabilities) are observed. The

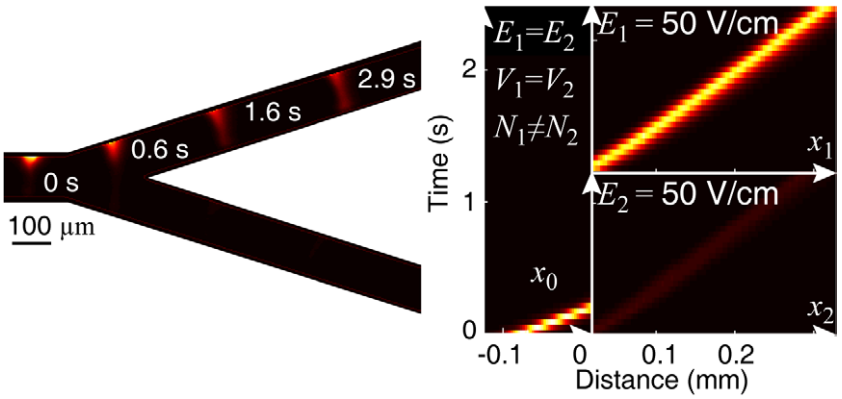

Figure 5. Experimental demonstration of the effect of electrokinetic fluctuations on sample splitting. Electric fields in the top and bottom channels are equal, but nominal electric field is high ($E = 100\,\mathrm{V\,cm^{-1}}$). On the left, the composite image shows the ITP sample zone at four successive times before, during and after bifurcation. Initially, the sample zone is not uniformly distributed along the channel width ($t = 0\,\mathrm{s}$), and is strongly skewed toward the top wall. Upon entering the bifurcation, the sample zone remains asymmetric ($t = 0.6\,\mathrm{s}$) and mostly exits into channel 1 ($t = 1.6\,\mathrm{s}$). A sample trace is just noticeable in the spatiotemporal plot of channel 2. The spatiotemporal plot also shows that most of the sample exits into 1, but that the sample zone velocities in channels in 1 and 2 remain equal (i.e. equal slopes), as predicted by equation (2).

system we consider here contains three or four ionic species per zone, has strong 3D effects, has a base state with non-uniform unsteady flow, etc.

We first qualitatively describe the effect of the EKI-type fluctuations on sample splitting. In the example experiment shown on figure 5, we established equal electric fields in channels 1 and 2. The composite image shows visualization of an ITP zone negotiating the bifurcation region at an electric field of the order of $100\,\mathrm{V\,cm^{-1}}$ in the main channel. At this field, samples showed fairly strong spanwise concentration gradients. In this example, the sample distribution is strongly asymmetric, with most of the sample focused on the upper part of the channel (in other realizations at the same conditions, the sample may focus mostly near the bottom wall). After passing the bifurcation, the sample is not effectively split. The images and spatiotemporal plot show that most of the sample enters the top channel. This strong initial asymmetry clearly affects the splitting process. Despite the inaccurate splitting of this experiment, we observe that the sample velocities remain the same in channels 1 and 2 after bifurcation (showing the symmetry of the applied fields and that equation (2) still holds).

We now more quantitatively explore deviations from the simple theory described earlier by analyzing measured values of the term $(N_2/N_1)(V_1/V_2)$ for about 100 splitting experiments. For stable flows (with no observed fluctuations in the shape and intensity of the approach ITP band), we note that the value of the splitting term $(N_2/N_1)(V_1/V_2)$ is consistently near unity as described in the inset of figure 3(b). To quantify the effect of high field and conductivity gradient in ITP splitting, we explored several methods of scaling data based on the hypothesis that these fluctuations in splitting ratio are due to EKI-type dynamics.

Electrokinetic instabilities occur when electric body forces are much larger than the viscous forces in the flow. Posner and Santiago [29] review a few scaling approximations for these electric body forces. We here propose a simple scaling for electric body force $\rho_e E$ at an ITP interface specifically. Applying Gauss' law to the LE/TE interface, we can scale the free charge density, ρ_e, as

$$\rho_e = -\varepsilon \nabla \cdot \mathbf{E} \sim (E_T - E_L)/\delta, \tag{4}$$

where ε is the dielectric constant of the fluid and δ is the characteristic ITP interface width. We (again) apply current conservation to express electric field ratio in terms of conductivity ratio and write

$$\rho_e E \sim E_{av} E_L (\gamma - 1)/\delta, \tag{5}$$

where we used the arithmetic average field at the interface $E_{av} = (E_L + E_T)/2 = E_L(1+\gamma)/2$. In terms of the average field only

$$\rho_e E \sim \frac{E_{av}^2}{\delta} \frac{(\gamma - 1)}{(\gamma + 1)}. \tag{6}$$

In typical EKI models of symmetric, binary electrolytes, the length scale of free charge regions is determined by the effects of convective-diffusion transport alone [32]. However, in (multispecies) ITP the characteristic interface width is due to a balance of electromigration and diffusion. In ITP, δ strongly depends on electric field and scales as $\sigma_L/j = 1/E_L$ (j is the current density) [13, 22], so our Coulombic force density scaling becomes

$$\rho_e E \sim E_{av}^3 \frac{(\gamma - 1)}{(\gamma + 1)^2}. \tag{7}$$

We therefore chose this to scale our data and for the abscissa of figure 6.[3] We stress that the stronger field dependence of this proposed, approximate scaling (i.e. E^3) relative to the typical E^2-type scaling of typical EKI studies [26, 29, 32] is due to the self-sharpening effect of ITP interfaces.

The result of our analysis is shown in figure 6. Figure 6(a) shows that the splitting ratio, $(N_2/N_1)(V_1/V_2)$, collapses to values near unity (within experimental uncertainty) for low values of the critical parameter $E_{av}^3(\gamma - 1)/(\gamma + 1)^2$, as expected. At values of $E_{av}^3(\gamma - 1)/(\gamma + 1)^2$ greater than about $15 \times 10^4\,\mathrm{V^3\,cm^{-3}}$ (for typical conductivity ratios, corresponding to electric fields of order $100\,\mathrm{V\,cm^{-1}}$) we see a sudden increase in the scatter about the stable value of $(N_2/N_1)(V_1/V_2) = 1$. This scatter in the values of $(N_2/N_1)(V_1/V_2)$ is due to the asymmetries created by flow instabilities on the bifurcation and splitting dynamics of the ITP zone.

Figure 6(b) shows evidence supporting the hypothesis that instability-induced asymmetries in the inlet channel (approaching the bifurcation) result in asymmetries in the splitting ratio. We quantify the anisotropy in the inlet channel using the parameter M_2/M_1; here defined as

[3] We note that internal pressure gradients generated by non-uniform EOF result in both strong axial and spanwise conductivity gradients. Santos and Storey [30] suggest that strong spanwise conductivity and spanwise electric field components are important for the onset of EKI in flows with initially strong axial conductivity gradients (as in ITP). In any case, we found qualitatively little difference between the current scaling and other forms of scaling reviewed by Posner and Santiago [29].

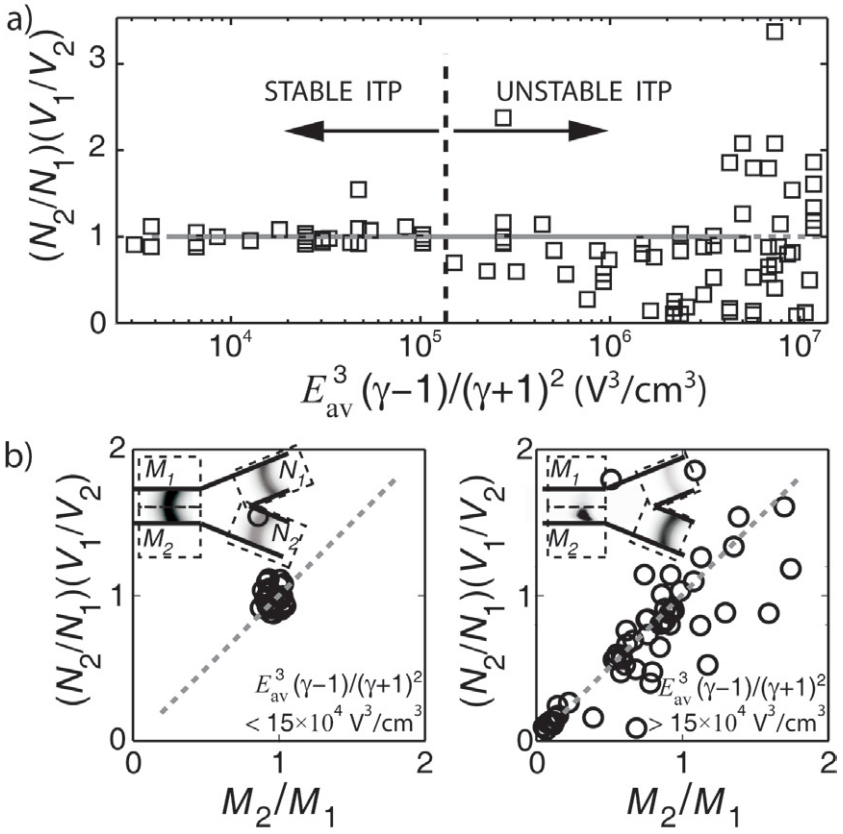

Figure 6. Regimes of stable and unstable ITP and ITP-based sample splitting. (a) Normalized splitting ratio $(N_2/N_1)(V_1/V_2)$ for increasing values of the parameter $E_{av}^3(\gamma-1)/(\gamma+1)^2$, which scales electric body forces that can cause destabilization of electrokinetic flows. Each of these 88 data points corresponds to a measurement of the splitting ratio normalized by the velocity ratio. TE's used are 100 mM Tris HEPES, 75 mM sodium TPB, or 100 mM sodium benzoate. At low values of $E_{av}^3(\gamma-1)/(\gamma+1)^2$, sample portions have $(N_2/N_1)(V_1/V_2)$ values of approximately 1. For values of $E_{av}^3(\gamma-1)/(\gamma+1)^2$ above about $15\times10^4\,V^3\,cm^{-3}$, we observe that the splitting ratio deviates from unity and scatter in the data increases dramatically. The associated deviations from unity show the breakdown of the Kirchoff-type law for sample splitting at high $E_{av}^3(\gamma-1)/(\gamma+1)^2$. (b) Effect of inlet channel sample anisotropy, M_2/M_1, on sample splitting. M_1 and M_2 are the total fluorescent intensity in respectively the top and the bottom half of the inlet channel (see inset schematic). On the left is the stable case ($E_{av}^3(\gamma-1)/(\gamma+1)^2 < 15\times10^4\,V^3\,cm^{-3}$) where the sample splitting is roughly symmetric so that $M_1\approx M_2$, and the normalized splitting ratio both cluster about unity (27 data points, average values $M_2/M_1 = 0.96$ and $(N_2/N_1)(V_1/V_2)=1$, with standard deviations of ~0.09). On the right are measurements of the unstable case where $E_{av}^3(\gamma-1)/(\gamma+1)^2 > 15\times10^4\,V^3\,cm^{-3}$. Here, the input anisotropy ratio deviates from unity but correlates with $(N_2/N_1)(V_1/V_2)$ ($R^2=0.84$). This correlation suggests that instability in the inlet channel causes the asymmetry in splitting.

ratio of the total fluorescence intensity in the bottom half of the channel, M_2, divided by that of the top half of the channel, M_1 (cf inset schematics in figure 6(b)). For the stable case ($E_{\mathrm{av}}^3(\gamma-1)/(\gamma+1)^2 < 15\times10^4\,\mathrm{V^3\,cm^{-3}}$), values of M_2/M_1 and $(N_2/N_1)(V_1/V_2)$ both consistently cluster near unity. Although difficult to resolve in the figure, we here show 27 stable data points and 26 of these are clustered to within about 10% of 1.0 (we note that there is one outlier shown which gave a split ratio of 1.5). On the right side of figure 6(b) are measurements in the unstable regime ($E_{\mathrm{av}}^3(\gamma-1)/(\gamma+1)^2 > 15\times10^4\,\mathrm{V^3\,cm^{-3}}$) which results in points roughly distributed over a (dashed) correlation line, $M_2/M_1 = (N_2/N_1)(V_1/V_2)$. Although there is some scatter (due to difficulties in capturing and quantifying accurately high-field, unstable ITP zone shapes), the data have a significant correlation ($R^2 = 0.84$) between the inlet anisotropy and outlet splitting ratio. Together with the qualitative image data, these data strongly suggest that anisotropy in the input channel causes the asymmetries in splitting. Lastly, the insets in figures 6(b), respectively, show actual images of a stable case resulting in a symmetric splitting (left) and an asymmetric split caused by instability in the inlet channel (right).

5. Conclusion

In this paper, we described a method to fairly efficiently and accurately split an ionic sample zone at a channel intersection by controlling buffer chemistry and electric potential. Buffer chemistry allows robust ITP focusing and preconcentration of the sample. Control of the applied electric potential along two outlet channels allows sample splitting. Despite the complex physics involved in the ITP zone splitting process, we showed that, at typical ITP conditions, the splitting follows a simple scaling based on Kirchoff's current conservation law. That is, we found that the sample split ratio (moles delivered to the first channel divided by moles delivered to the second channel) equals the first-to-second-channel ionic current ratio. We verified this rule across buffer chemistries and absolute values of electric fields.

We also reported observations of spatiotemporal fluctuations of the ITP interface at sufficiently high electric fields. We attributed these fluctuations to electrokinetic instabilities. We showed a correlation between onset of instability in the inlet channel and breakdown of the simple splitting rule at large field and conductivity ratios. We found the scaling $E_{\mathrm{av}}^3(\gamma-1)/(\gamma+1)^2$ provides an adequate description of the onset of instabilities in this flow. For our channel system, we found a value of $E_{\mathrm{av}}^3(\gamma-1)/(\gamma+1)^2 = 15\times10^4\,\mathrm{V^3\,cm^{-3}}$ adequately delineates stable and unstable regimes in our flow field. For typical conductivity ratios ranging from 2 to 10, this translates to an electric field magnitude of $100\,\mathrm{V\,cm^{-1}}$. However, we note that the electric body force scale value is likely to be dependent on device-specific factors such as geometry, ion diffusivities and mobilities, and electroosmotic flow mobility. Also, we note that high electric field is often applied to reduce migration time in anionic ITP. To avoid instabilities and achieve accurate sample splitting at bifurcations, we suggest reducing EOF and maintaining electric fields within a 'safe' range, which avoids EKI. There is abundant literature on EOF reduction methods [33, 34].

With some minor constraints on chemistry and electric field magnitude, ITP sample zone splitting and control seems a robust, accurate and easy to implement technique. In future work, we hope to further resolve our scaling and instability analyses for ITP. We also hope to apply stable-regime splitting techniques to multidimensional ITP separation assays, multiple ITP sample extractions and/or sample delivery to reactor arrays.

Acknowledgment

This work was sponsored by Ebara Corporation, Tokyo, Japan.

References

[1] Maerkl S J and Quake S R 2007 *Science* **315** 233–7
[2] Ottesen E A, Hong J W, Quake S R and Leadbetter J R 2006 *Science* **314** 1464–7
[3] Thorsen T, Maerkl S J and Quake S R 2002 *Science* **298** 580–4
[4] Emrich C A, Tian H J, Medintz I L and Mathies R A 2002 *Anal. Chem.* **74** 5076–83
[5] Tian H J, Emrich C A, Scherer J R, Mathies R A, Andersen P S, Larsen L A and Christiansen M 2005 *Electrophoresis* **26** 1834–42
[6] Adamson D N, Mustafi D, Zhang J X J, Zheng B and Ismagilov R F 2006 *Lab Chip* **6** 1178–86
[7] Link D R, Anna S L, Weitz D A and Stone H A 2004 *Phys. Rev. Lett.* **92** 054503
[8] Roman G T, Wang M, Shultz K N, Jennings C and Kennedy R T 2008 *Anal. Chem.* **80** 8231–8
[9] Das C, Zhang J, Denslow N D and Fan Z H 2007 *Lab Chip* **7** 1806–12
[10] Griffiths S K and Nilson R H 2001 *Anal. Chem.* **73** 272–8
[11] Zhuang Z X and Jacobson S C 2009 *Anal. Chem.* **81** 1477–81
[12] Bocek P 1981 *Analytical Problems (Topics in Current Chemistry)* (Berlin: Springer) pp 131–77
[13] Khurana T K and Santiago J G 2008 *Anal. Chem.* **80** 6300–7
[14] Gebauer P and Bocek P 1995 *Electrophoresis* **16** 1999–2007
[15] Moore G T 1975 *J. Chromatogr.* **106** 1–16
[16] Nee T W 1974 *J. Chromatogr.* **93** 7–15
[17] Jung B, Bharadwaj R and Santiago J G 2006 *Anal. Chem.* **78** 2319–27
[18] Jung B G, Zhu Y G and Santiago J G 2007 *Anal. Chem.* **79** 345–9
[19] Pospichal J, Gebauer P and Bocek P 1989 *Chem. Rev.* **89** 419–30
[20] Khurana T K and Santiago J G 2008 *Anal. Chem.* **80** 279–86
[21] Cui H C, Dutta P and Ivory C F 2007 *Electrophoresis* **28** 1138–45
[22] Saville D A and Palusinski O A 1986 *AIChE J.* **32** 207–14
[23] Bercovici M, Lele S K and Santiago J G 2009 *J. Chromatogr.* A **1216** 1008–18
[24] Saville D A 1990 *Electrophoresis* **11** 899–902
[25] Khurana T K and Santiago J G 2009 *Lab Chip* **9** 1377–84
[26] Baygents J C and Baldessari F 1998 *Phys. Fluids* **10** 301–11
[27] Hoburg J F and Melcher J R 1976 *J. Fluid Mech.* **73** 333–51
[28] Lin H, Storey B D, Oddy M H, Chen C H and Santiago J G 2004 *Phys. Fluids* **16** 1922–35
[29] Posner J D and Santiago J G 2006 *J. Fluid Mech.* **555** 1–42
[30] Santos J J and Storey B D 2008 *Phys. Rev.* E **78** 015301
[31] Oddy M H and Santiago J G 2005 *Phys. Fluids* **17** 064108
[32] Chen C H, Lin H, Lele S K and Santiago J G 2005 *J. Fluid Mech.* **524** 263–303
[33] Horvath J and Dolnik V 2001 *Electrophoresis* **22** 644–55
[34] Righetti P G, Gelfi C, Verzola B and Castelletti L 2001 *Electrophoresis* **22** 603–11